Int. J. Metrol. Qual. Eng. **17**, 14 (2026)
© L. Xu, Published by EDP Sciences, 2026
https://doi.org/10.1051/ijmqe/2026014

**International Journal of Metrology and Quality Engineering**

Available online at:
www.metrology-journal.org

Research Article — Open Access

# Construction of a reliability assessment model for railway cable-stayed bridges based on WSN real-time sensing and MISSA-SVM collaboration

Liyan Xu*

School of Rail Transit, Anhui University of Applied Technology, Hefei, 230011, PR China

Received: 23 January 2026 / Accepted: 2 June 2026

**Abstract.** To better assess the reliability of railway cable-stayed bridges (CSBs), this paper proposes a reliability assessment model that integrates wireless sensor networks with a multi-strategy improved sparrow search algorithm and support vector machine collaboration. A hierarchical wireless sensor network sensing system is built, a support vector machine penalty factor is introduced, and the multi-strategy improved sparrow search algorithm is used for optimization. Verification experiments were carried out based on standard test functions, node deployment simulations, and bridge-measured data, and the data related to fitting accuracy were based on the data generated by the finite element simulation model as the real value. The results showed that after the model optimization, the node coverage of the wireless sensor network reached 82%, the average absolute error of the main tower stress fitting is only 0.32 MPa, and the total computation time for 250 sets of samples is 51.5 s. The proposed model can achieve efficient dynamic assessment of the structural state of railway CSBs, providing technical support for intelligent bridge operation and maintenance.

**Keywords:** Railway cable-stayed bridge / reliability assessment / wireless sensor network / sparrow search algorithm / support vector machine

## 1 Introduction

The reliability of railway cable-stayed bridges (CSBs) is widely used in railway transportation engineering in complex terrain, and their structural reliability directly determines the safety of railway transportation [1]. The reliability assessment of traditional railway CSBs mostly relies on manual inspection and fixed-point instrument monitoring, which has inherent drawbacks such as high labor costs and inefficient dynamic response [2]. Wireless sensor networks (WSNs) have become the core technical means for bridge structure monitoring due to their core advantages, such as distributed deployment and real-time data acquisition. Yang et al. introduced a bridge WSN clustering routing algorithm grounded in multi-criteria decision-making. This algorithm optimized network communication efficiency but did not conduct in-depth research on WSN data noise processing [3]. In the field of evaluation algorithms, support vector machine (SVM) is widely used in structural reliability prediction scenarios, but it needs to be combined with optimization algorithms for parameter calibration [4]. The sparrow search improved algorithm based on multi-strategy (MISSA) algorithm, as a new type of intelligent optimization algorithm, has shown significant advantages in the field of engineering optimization [5]. Chen and Sun proposed a multi-strategy improved sparrow search algorithm (SSA) based on the first definition of ellipse. The algorithm effectively improved the global optimization ability through dual-strategy fusion [6]. Chen et al. combined MISSA with the Gaussian pyramid model to construct a science fiction painting similarity detection method. Their experimental results verified the adaptability of MISSA in multiple tasks [7]. In the dimension of bridge condition assessment, Cukaci and Soyoz proposed a vision-based cable force identification method for CSBs, which realized the accurate monitoring of key mechanical indicators of bridges [8].

Existing research indicates insufficient integration between WSN and evaluation algorithms, lacking an integrated solution that simultaneously addresses node deployment optimization, data denoising, and algorithm parameter calibration. Therefore, this study proposes a railway CSB reliability evaluation model that combines real-time WSN sensing with MISSA-SVM collaboration, aiming to solve the problems of low accuracy, poor timeliness, and insufficient algorithm parameter optimi-

* Corresponding author: xly_hf@163.com

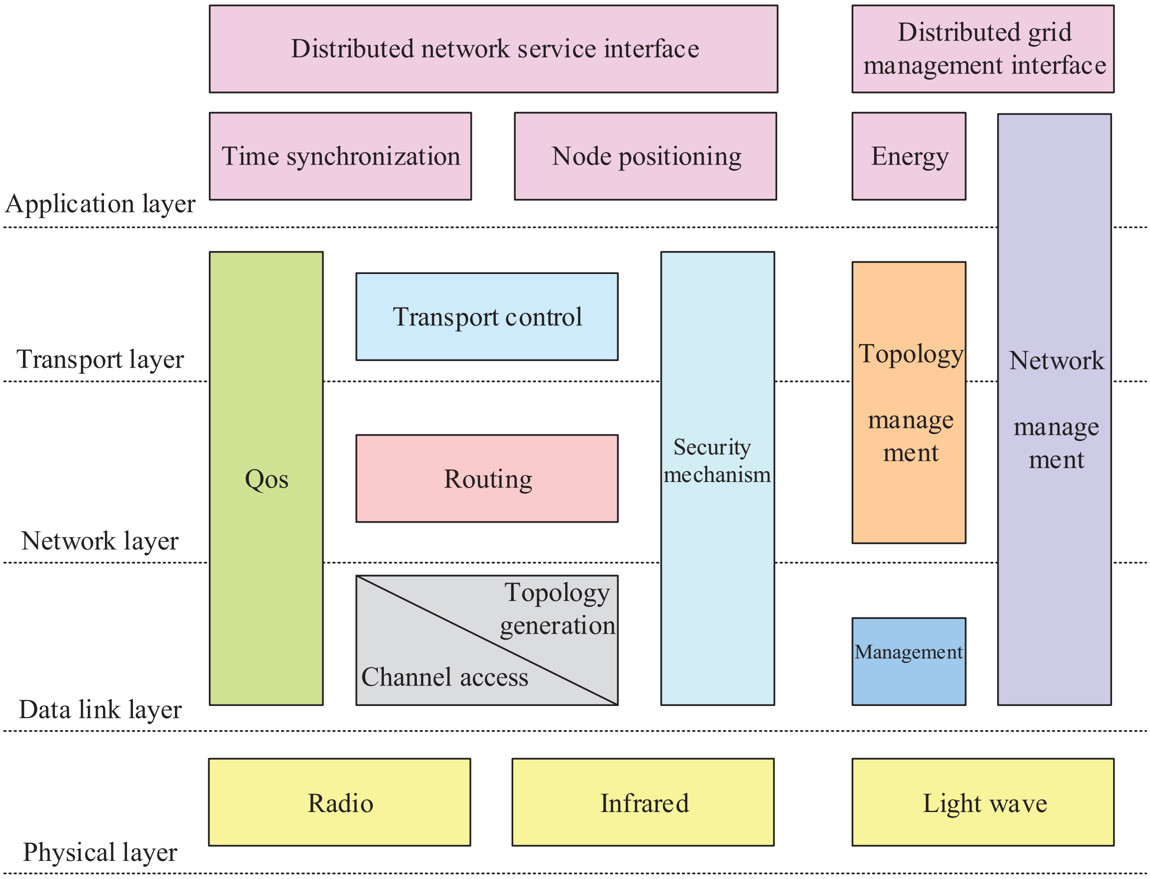


**Fig. 1.** Schematic diagram of WSN node architecture.

zation in traditional evaluation methods. The innovation lies in the deep integration of the MISSA with WSN and SVM, constructing an integrated evaluation system adaptable to complex service environments, balancing evaluation accuracy and real-time requirements.

## 2 Methodology

### 2.1 Construction of real-time sensing model for railway CSBs based on WSN

WSN refers to a distributed sensor network, with its terminal nodes being sensors capable of sensing and monitoring the external environment [9]. In WSNs, sensors utilize wireless communication, enabling a highly flexible network configuration where device positions can be adjusted freely as needed, and it is capable of establishing a connection to the Internet via wired or wireless means [10]. The node structure of WSN is presented in Figure 1.

As shown in Figure 1, the WSN node architecture adopts a layered design. From the bottom layer to the top layer, each layer has a clear function and works together. At the same time, it integrates security mechanisms and network management modules. The physical layer is accountable for data transmission through media such as radio and infrared; the data link layer completes channel access and topology generation; the network layer provides routing and QoS guarantee; the transmission layer realizes reliable end-to-end transmission; and the application layer is oriented towards specific services, providing functions such as time synchronization and node positioning [11]. Based on the WSN node architecture, this study combines the monitoring needs of railway CSBs under multiple factors such as train load, environmental erosion, and structural aging and constructs a targeted real-time perception model, which can realize full-dimensional and high-precision perception of bridge structure status and surrounding environmental parameters. The real-time perception model of railway CSB based on WSN is shown in Figure 2.

As shown in Figure 2, the selection and optimization of the sensing module focuses on the special needs of bridge monitoring. The sensor selection prioritizes high precision, anti-interference, and adaptability to harsh environments. MEMS vibration acceleration sensors, temperature sensors, humidity sensors, and other equipment are selected to accurately capture the vibration response and environmental impact parameters of the railway CSB [12]. At the same time, in view of the service requirements of long-term monitoring of railway CSBs, the nodes adopt a low-power design scheme. By optimizing the hardware selection and communication protocol, the service time of the nodes is effectively extended and the maintenance cost is reduced. The data acquisition and preprocessing mechanism takes real-time performance and reliability as the core objectives: the acquisition stage sets a differentiated acquisition

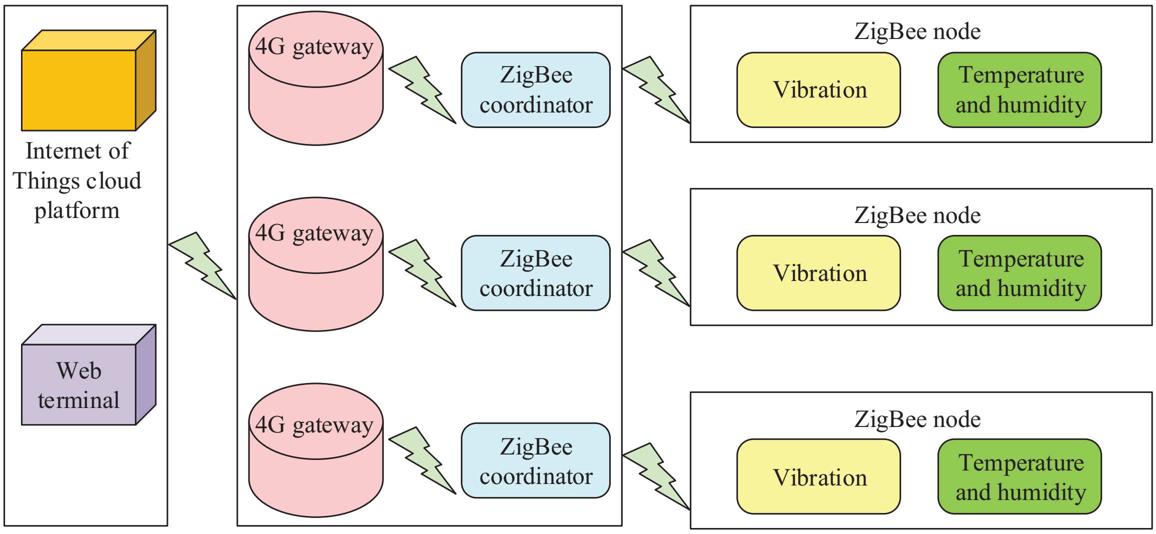


**Fig. 2.** Real-time perception model of railway CSB based on WSN.

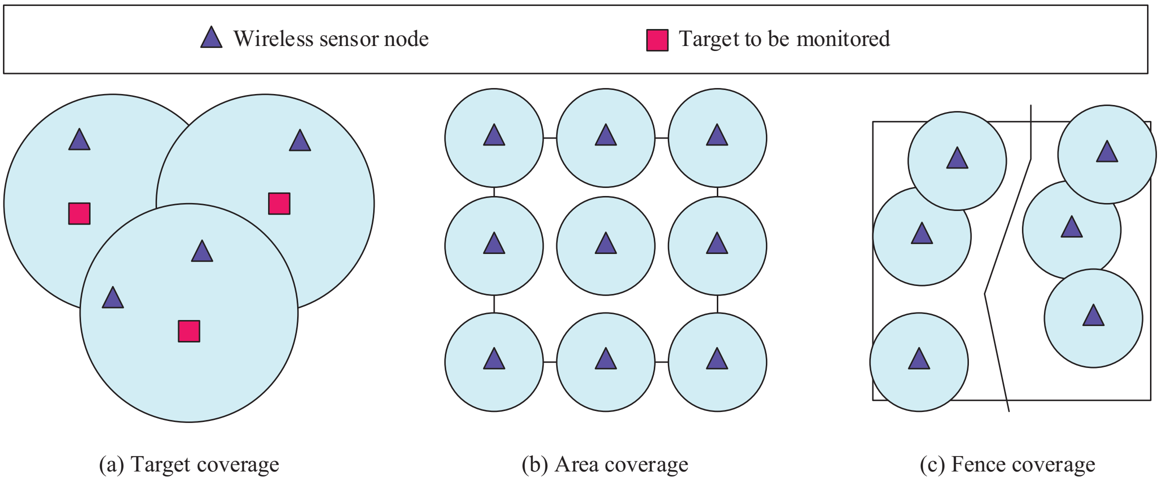


**Fig. 3.** Types of WSN coverage problems.

frequency based on the importance of the monitoring parameters, uses a ZigBee self-organizing network to realize low-power real-time transmission between terminal nodes and acquisition equipment, and uses a 4G gateway module to complete high-speed data upload and cloud access. In the preprocessing stage, a series of methods such as noise reduction, outlier removal, data standardization, and feature extraction are used to eliminate the impact of environmental interference and equipment error on data quality, and the effectiveness verification ensures that the preprocessed data can accurately reflect the structural state of the railway CSB [13]. Given the complexity and variability of WSN application environments, coverage issues can be categorized from multiple dimensions. Common WSN coverage problem types are shown in Figure 3.

Figure 3a shows target coverage. This type of coverage focuses on the monitoring of specific key targets and the precise coverage of one or more key monitoring points. The core requirement is to ensure the integrity and timeliness of the monitoring data of the target area. Figure 3b shows area coverage. Its core objective is to achieve full coverage of the designated monitoring area, ensure that there are no blind spots in the area, and meet the requirements of overall structural status assessment. Figure 3c shows fence coverage. This type belongs to boundary monitoring coverage. Its function is to construct a virtual monitoring boundary and achieve precise detection of the behavior of target objects crossing the boundary [14]. On a two-dimensional surface, a sensor node (SN)'s detection area forms a circle centered on the node, with a radius of $R$. This circular area is usually called the sensing disk of the node and $R$ is called the sensing radius of the SN. The sensing radius is related to the physical characteristics of the built-in sensor device of the node. Assume that the position coordinates of the SN $n$ are $(x_n,\, y_n)$ in the sensing model. The Euclidean distance between the SN and the monitoring node is shown in equation (1).

$$d(n,t) = \sqrt{(x_n - x_t)^2 + (y_n - y_t)^2}. \tag{1}$$

In equation (1), $t$ represents the monitoring node, and $(x_t, y_t)$ represent the coordinates of the monitoring node. The expression for the node $n$'s perception probability $p_n(t)$ of the target point $t$ is shown in equation (2).

$$p_n(t) = \begin{cases} 1, & \text{if } d(n,t) \le R; \\ 0, & \text{if } d(n,t) > R. \end{cases} \tag{2}$$

The expression for the joint perception probability $p_{\text{joint}}(t)$ of all SNs of target point $t$ is shown in equation (3).

$$p_{\text{joint}}(t) = 1 - \prod_{i=1}^{m} [1 - p_{ni}(t)]. \tag{3}$$

In equation (3), $m$ is the total number of SNs, $i$ represents traversing all SNs, and $p_n(t)$ represents the probability that the $i$th SN can detect the target point $t$ alone [15]. The expression for the overall coverage rate $V$ is shown in equation (4).

$$V = \frac{\sum_{x=1}^{L} \sum_{y=1}^{W} p_{\text{joint}}(t)}{L \times W}. \tag{4}$$

In equation (4), $L$ and $W$ represent the number of rows and columns of the grid.

## 2.2 Construction of a reliability assessment model for railway CSBs integrating WSN and MISSA-SVM

To improve the real-time performance and accuracy of the structural state perception of railway CSBs, a real-time perception model for railway CSBs based on WSN is proposed. To further optimize the coverage performance and energy efficiency of WSN and improve the accuracy of subsequent structural reliability assessment, MISSA is introduced to optimize the core parameters of the perception model. MISSA is based on the standard SSA framework and uses iterative mapping to generate chaotic sequences to complete the population initialization [16]. The chaotic value $x_{k+1}$ of the $k+1$ th iteration is calculated as shown in equation (5).

$$x_{k+1} = \sin\frac{\alpha\pi}{x_k}. \tag{5}$$

In equation (5), $x_k$ is the chaos value of the $k$th iteration and $\alpha$ is the control parameter [17]. The MISSA achieves a balance between the algorithm's ability to explore globally and exploit locally by dynamically adjusting the ratio of the two, and the calculation formula of its proportional control coefficient is shown in equation (6).

$$r = h\cdot\tan\left(\frac{\pi}{3} - \frac{\pi}{3}\cdot\left(\frac{q}{q_{Max}}\right)\right) + o\cdot\text{rand }(0.1). \tag{6}$$

In equation (6), $h$ represents the proportional control coefficient, $q$ is the current iteration number, $q_{max}$ is the max iteration number, $o$ represents the disturbance deviation factor, and rand (0,1) is a random variable. The formulas for calculating the number of leaders PDNum and the number of followers SDNum are shown in equation (7).

$$\begin{cases} \text{PDNum} = r\cdot\text{SearchAgents} \\ \text{SDNum} = (1-r)\cdot\text{SearchAgents} \end{cases}. \tag{7}$$

In equation (7), SearchAgents represents the population size. The leader position update strategy of SSA has the defects of fixed search step size and poor adaptability to environmental changes. When facing complex optimization problems with high dimension and multiple constraints such as WSN node deployment, it is easy to have low search efficiency or premature convergence [18]. The MISSA improves the leader's ability to guide the global optimal solution by introducing dynamic step size adjustment and environmental awareness factor. The position update formula of the $a$th individual in the $k$th generation in the $b$th dimension is shown in equation (8).

$$X_{a,b}^{k+1} = \begin{cases} X_{a,b}^{k}\cdot\left[\exp\left(\frac{2i}{\beta\cdot k_{\text{Max}}}\right)\right] & R_2 < \text{ST}, \\ X_{a,b}^{k}\cdot Q\cdot M & R_2 \ge \text{ST}. \end{cases} \tag{8}$$

In equation (8), β is a random parameter, and its threshold is selected based on the optimization requirements of WSN node deployment. The value range is [0,1]; $R_2$ is an early warning value, and its threshold selection is determined based on the changing characteristics of the population fitness during the algorithm iteration process, and its value range is [0,1]. When $R_2 < 0.5$, the population is judged to be in a safe search state, and the leader updates the position according to the normal strategy. When $R_2 \ge 0.5$, it is judged that there is a local optimal risk, and the dynamic step adjustment mechanism is triggered to improve the global search capability; ST is a safety threshold, $Q$ is a random step size, and $M$ is a matrix of all 1s. The search ability of the follower directly determines the local development accuracy of the algorithm. In SSA, the follower simply follows the leader's movement, which easily leads to the search getting trapped in a local optimum (LO) [19]. The follower position update formula of the MISSA is shown in equation (9).

$$X_{a,b}^{k+1} = \begin{cases} X_{a,b}^{k} + r_1\cdot\sin(r_2)\cdot|r_3\cdot X_{\text{best}}^{k} - X_{a,b}^{k}| & r_4 \le 0.5, \\ {}_{a,b}^{k} + r_1\cdot\cos(r_2)\cdot|r_3\cdot X_{\text{best}}^{k} - X_{a,b}^{k}| & r_4 > 0.5. \end{cases} \tag{9}$$

In equation (9), $X_{\text{best}}^{k}$ represents the current global optimal position, $r_1$ is the search range control parameter, $r_2$ represents the movement distance determination parameter, $r_3$ represents the target scaling parameter, and $r_4$ represents the sine/cosine selection parameter. The expression for the search range control parameter $r_1$ is shown in equation (10).

$$r = 1.5 - \left(\frac{a}{k_{\text{Max}}}\right)^3. \tag{10}$$

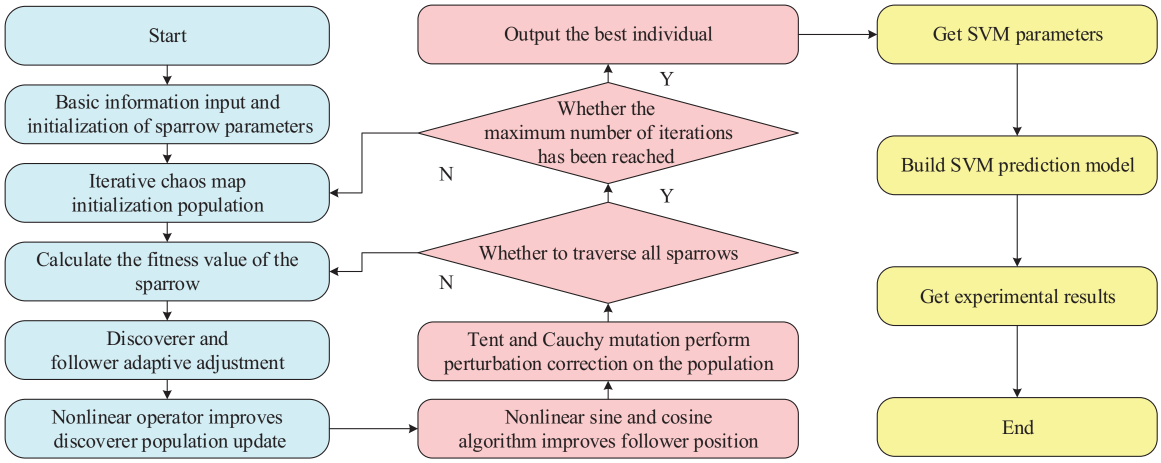


**Fig. 4.** Flowchart of MISSA-SVM algorithm.

To further avoid the algorithm from getting stuck in an LO in the later stage of iteration and improve the diversity of the population, the study conducted chaotic perturbation on the individuals in the population after each iteration. Considering that the Tent chaotic map has the characteristics of good ergodicity and fast convergence speed but also has the defects of a short period and ease of getting stuck in small-period oscillation, the study introduced random variables to modify the original tent map in order to enhance the randomness and ergodicity of the chaotic sequence [20]. The modified tent chaotic map expression is shown in equation (11).

$$\mathrm{Tent}_{a+1} = \begin{cases} \dfrac{\mathrm{Tent}_a}{2} + \dfrac{1}{N} \times \mathrm{rand}(0,1), & 0 < \mathrm{Tent}_a \le 0.5; \\ 2(1 - \mathrm{Tent}_a) + \dfrac{1}{N} \times \mathrm{rand}(0,1), & 0.5 < \mathrm{Tent}_a \le 1. \end{cases} \tag{11}$$

In equation (11), $\mathrm{Tent}_a$ represents the $a$th chaotic sequence value, and $N$ represents the number of particles in the chaotic sequence. A Bernoulli shift transformation is then performed on the individual particles after the chaotic perturbation, and the transformed expression is shown in equation (12).

$$\mathrm{Tent}_{a+1} = (2 \times \mathrm{Tent}_a) mod\, 1 + \frac{1}{N}\mathrm{rand}(0,1). \tag{12}$$

Furthermore, to enhance population diversity and algorithm robustness, a Cauchy mutation strategy was introduced after chaotic perturbation to mutate some individuals, thereby breaking free from the constraints of local optima. The Cauchy mutation formula is shown in equation (13).

$$Mutation(x) = x \times [1 + u \times \tan(\pi \times (\mathrm{rand}(0,1) - 0.5))]. \tag{13}$$

In equation (13), $u$ represents the variation intensity coefficient. To achieve an accurate assessment of the structural reliability of railway CSBs, after optimizing the core parameters of the WSN perception model through MISSA and obtaining high-quality structural condition perception data, the study further introduces SVM to build a reliability assessment model. SVM is a generalized linear classifier that performs binary classification of data in a supervised learning manner. Its decision boundary is the maximum margin hyperplane that solves the learning sample. Combined with the nonlinear characteristics of railway CSB structural monitoring data, the study selects the radial basis function as the kernel function of SVM. This kernel function has the advantages of strong generalization ability, adaptability to high-dimensional data, and flexible parameter adjustment. It can effectively fit nonlinear monitoring indicators such as bridge main tower stress and main beam deflection. At the same time, in the process of optimizing the SVM penalty factor, MISSA simultaneously performs collaborative optimization of the kernel parameter $\gamma$ of the radial basis function and determines the optimal combination of the penalty factor and the kernel parameter $\gamma$ through the global optimization capability of the algorithm to avoid insufficient model fitting accuracy or overfitting problems caused by single parameter optimization. The flowchart of the MISSA-SVM algorithm is shown in Figure 4.

As shown in Figure 4, the algorithm first enters the initialization stage, followed by initializing the sparrow population using an iterative chaotic mapping strategy. After initialization, the fitness value of each individual sparrow is calculated. Grounded in the fitness value, the population is divided into discoverers and followers, with discoverers responsible for expanding the search space and followers relying on discoverer information for local searches. A nonlinear operator is proposed to enhance the update mechanism of the discoverer population and enhance global search capabilities, while a nonlinear sine and cosine algorithm is used to optimize the follower position update strategy. The population is perturbed and corrected by combining tent mapping and Cauchy mutation to enrich population diversity. Then, the iteration termination condition is checked. If not all sparrows have been traversed, the fitness value calculation

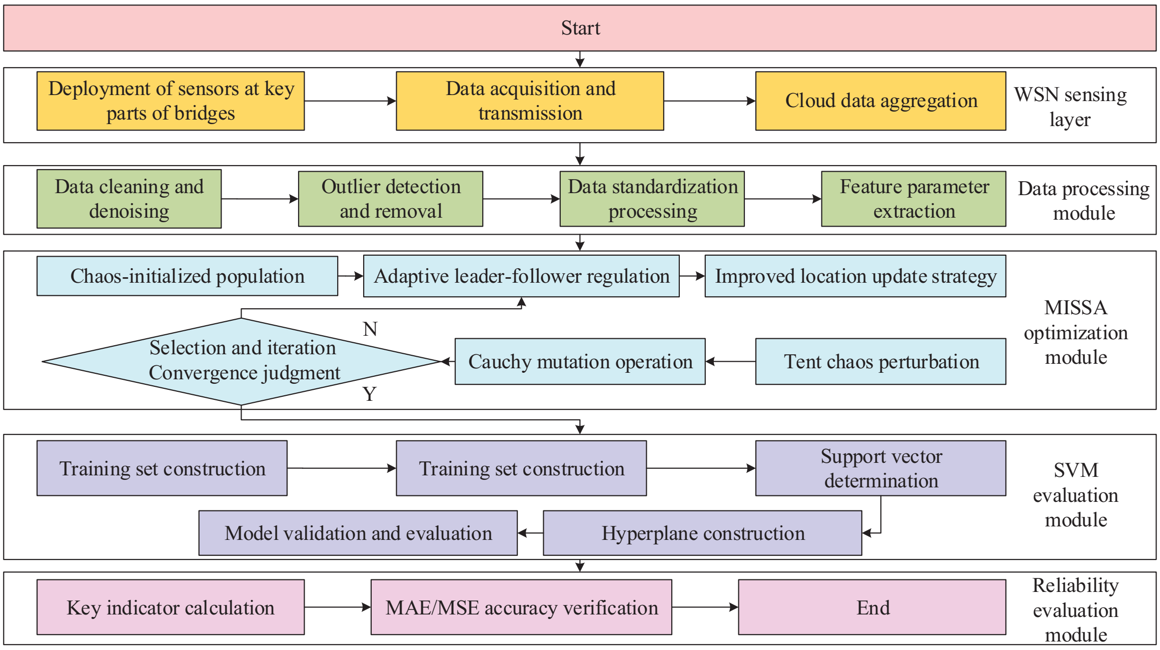


**Fig. 5.** Flowchart of the reliability assessment model for railway CSBs integrating WSN and MISSA-SVM.

step is returned; if the preset maximum number of iterations has not been reached, the population update and perturbation process is repeated until the termination condition is met. After iteration, the optimized SVM parameters are output, and an SVM prediction model is constructed based on these parameters. The final experimental results are obtained by substituting experimental data into the model. The flowchart of the reliability assessment model for railway CSBs integrating WSN and MISSA-SVM is shown in Figure 5.

As shown in Figure 5, the model constructs a real-time sensing system based on a WSN. MEMS sensors for vibration acceleration, temperature, and humidity are deployed in key components such as bridge cables, main beams, and towers. Data is collected and uploaded to the cloud via a ZigBee self-organizing network and a 4G gateway for low-power operation. After preprocessing, including denoising, outlier removal, standardization, and feature extraction, high-quality structural status data is output. Second, MISSA is used to optimize the core parameters of the WSN. Diverse populations are generated through chaotic initialization, adaptively adjusting the leader-follower ratio. Combined with an improved position update strategy and tent chaotic perturbation and Cauchy mutation operations, the spatial distribution of nodes is optimized, improving regional coverage and energy efficiency, providing accurate data support for the assessment. Finally, the optimized data is input into an SVM model. The model is trained using finite element simulation data as a benchmark, accurately fitting key indicators such as main beam deflection, main tower stress, and cable tension. The fitting accuracy is verified using mean absolute error (MAE) and mean squared error (MSE), while ensuring computational efficiency. The final bridge reliability assessment results are then output.

## 3 Experiments

The reliability assessment of railway CSBs adopted a comprehensive method of perception-fitting-judgment, based on WSN real-time perception data and MISSA-SVM model fitting and combining key indicators to complete structural reliability determination, forming a complete and verifiable evaluation system. The evaluation index selected the bridge core structure response index and the sensing system performance index. The first was the structural mechanics index, covering the main tower stress, the main beam mid-span deflection, and the cable tension, which reflected the load-bearing status of the bridge structure. The second was the sensing coverage index, that is, the WSN node coverage rate, which ensured the integrity of the monitoring data. The third was the fitting accuracy index, which was measured by MAE, MSE, and $R^2$ to ensure the accuracy of the index fitting. The study optimized WSN node deployment and SVM parameters through MISSA, improved perception and fitting performance, and completed reliability level determination based on various indicator thresholds to achieve accurate assessment of bridge structure status and adapt to high-speed railway bridge operation and maintenance needs.

### 3.1 Performance testing of the fusion WSN and MISSA-SVM algorithms

To fully verify the superiority of the MISSA-SVM algorithm, the grey wolf optimizer (GWO), butterfly optimization algorithm (BOA), and particle swarm optimization (PSO) algorithms were selected as control algorithms, and performance comparison experiments were conducted using standard test functions. The convergence

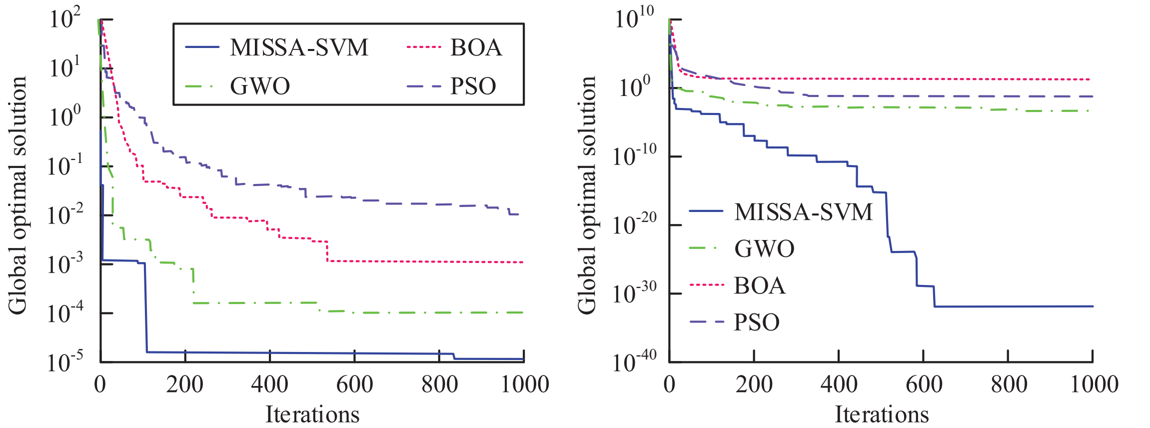


(a) Convergence curve on a unimodal test function (b) Convergence curve on multi-modal test function

**Fig. 6.** Convergence curves on unimodal/multimodal test functions.

factor of the GWO algorithm ranged from 2 to 0, and the random numbers were evenly distributed across the range from 0 to 1. The inertia weight of the PSO algorithms was set to 0.729, and both the individual learning factor and the swarm learning factor were set to 1.49445. The switching probability of the BOA was 0.6, the perception probability was 0.1, the control parameter was 0.01, and the random numbers were evenly distributed across the range from 0 to 1. The experiment used unimodal and multimodal functions to verify the convergence characteristics of the algorithm. The dimension of both types of functions was set to 30, with the unimodal function ranging from −1.28 to 1.28 and the multimodal function ranging from −5.12 to 5.12. The experimental environment configuration was as follows: the Intel Core(TM) i7-7500U processor, 4GB of memory, and the simulation platform were built based on Matlab 2021b. The convergence curves of the algorithm on the unimodal and multimodal test functions were shown in Figure 6.

Figure 6a showed the convergence curve on the unimodal test function. From Figure 6a, the MISSA-SVM algorithm exhibited a rapid decline trend in the early stage of iteration, entering a stable convergence phase in only about 110 iterations, and finally, the global optimal solution stabilized at the order of $10^{-5}$. Figure 6b showed the convergence curve on the multimodal test function. From Figure 6b, the MISSA-SVM algorithm continuously sought deep optimization during the iteration process, and finally the global optimal solution reached the order of $10^{-30}$. The convergence curves of the two types of test functions together showed that the MISSA-SVM algorithm had better convergence characteristics and optimization performance in both unimodal and multimodal problems. The standard SSA was selected as the control algorithm in this research, and comparative tests were performed around the node spatial distribution characteristics. The specific parameters were presented in Table 1.

Node deployment spatial distribution and coverage were core indicators for measuring WSN sensing capabilities. To intuitively compare the optimization effects of SSA and MISSA-SVM on node deployment, a node deployment

**Table 1.** Parameter settings.

| Parameter | Numerical value |
|---|---|
| Area | 100 × 100 × 100 |
| Number of nodes | 40 |
| Perception radius | 20 |
| Communication radius | 40 |
| Iteration count | 50 |

simulation experiment was conducted in a 100 × 100 × 100 three-dimensional monitoring area as the test scenario. The research expanded the two-dimensional sensing disk into a three-dimensional sensing sphere, extended the Euclidean distance formula to three-dimensional coordinate calculations, and replaced the number of grid rows and rows in the overall coverage formula with the number of three-dimensional space grids to achieve three-dimensional coverage quantification. The study focused on key load-bearing components such as main towers, main beams, and cables, ignoring redundant spaces in non-load-bearing parts. The spatial distribution of key components can be equivalent to a uniform 3D area, and node deployment is only for key components, which is in line with the simplification principle of bridge health monitoring engineering and takes into account pertinence and rationality. The node distribution and coverage of SSA-WSN were shown in Figure 7.

Figure 7a showed the node distribution of SSA-WSN. As can be seen from Figure 7a, the nodes were distributed in three-dimensional space as blue scattered dots, exhibiting an irregular characteristic of local dense clustering and global discrete distribution. Figure 7b showed the coverage rate of SSA-WSN nodes. From Figure 7b, the coverage rate increased rapidly in the early stage of iteration. When the number of iterations reached 13, the coverage rate no longer changed significantly and eventually stabilized at 71.6%, indicating that the traditional SSA had a fast

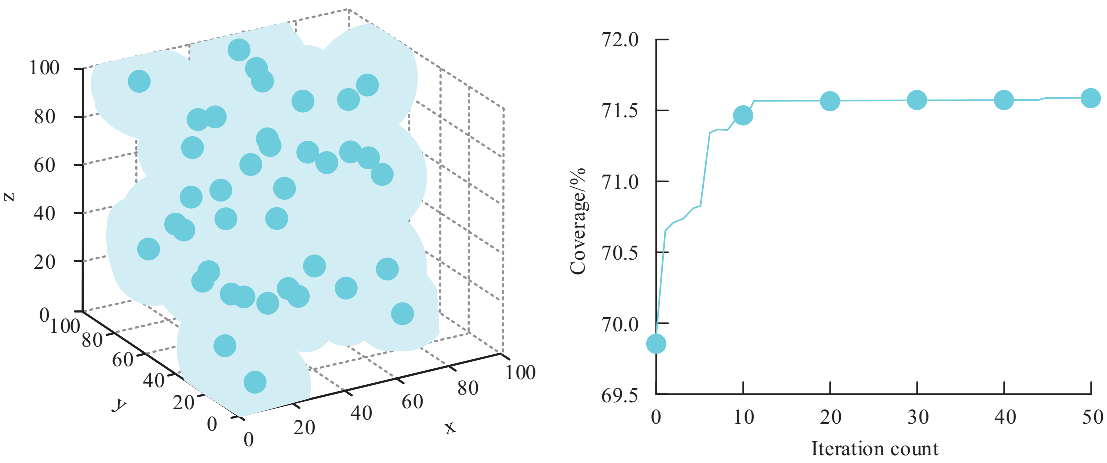


(a) SSA-WSN node distribution (b) Coverage of SSA-WSN nodes

**Fig. 7.** Distribution and coverage of SSA-WSN nodes.

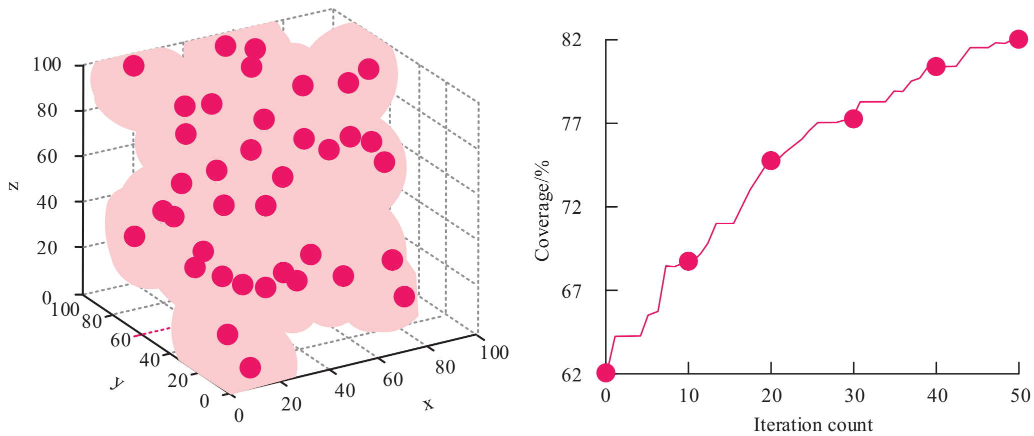


(a) MISSA-SVM-WSN node distribution (b) Coverage of MISSA-SVM-WSN nodes

**Fig. 8.** MISSA-SVM-WSN node distribution and coverage.

convergence speed but limited optimization accuracy. The node distribution and coverage rate of MISSA-SVM-WSN were shown in Figure 8.

Figure 8a showed the node distribution of MISSA-SVM-WSN. As shown in Figure 8a, the nodes were represented by pink scattered dots. There were no obvious dimensional coverage gaps in the X, Y, and Z dimensions, achieving full coverage of the preset monitoring area. Figure 8b showed the coverage rate of the MISSA-SVM-WSN nodes. As shown in Figure 8b, the coverage rate steadily increased with the number of iterations, without early convergence. When the iteration reached 50 times, the node coverage rate reached 82%. Therefore, the MISSA-SVM algorithm was more suitable for WSN deployment scenarios with high sensing performance requirements than the traditional SSA.

### 3.2 Performance testing of the reliability assessment model for railway CSBs integrating WSN and MISSA-SVM

In the complex service environment of bridges, the accuracy and stability of data transmission were prerequisites for the efficient operation of the monitoring system. To ensure the smooth progress of subsequent reliability assessment, the study first conducted communication performance tests on the optimized WSN. A high-speed railway concrete CSB was chosen as the test object. This bridge had a main span of 320 m, a main tower height of 120 m, and a service life of 8 years. The test area covered key monitoring points such as the mid-span of the main beam, the lower middle part of the main tower, and the anchorage ends of the cable stays. A total of 20 SNs were deployed, using a distributed layout, with a communication radius set at 50 m to meet the monitoring needs of the bridge's large span and multiple structures. In the wireless data transmission test, packet loss rate and received signal strength indicator (RSSI) were selected as evaluation indicators. During the test, the single data packet length was set to 100 bytes, the total number of data packets was 1000, and the sampling frequency was 10 Hz. Eight repeated tests were conducted under the complex service environment of the bridge under normal traffic conditions, with each test lasting 100 s. The measured packet loss rate and signal strength data were presented in Table 2.

**Table 2.** Packet loss rate and signal strength test.

| Frequency | Number of received data packets | Packet loss count | Packet loss rate (%) | Signal strength (dBm) |
|---|---|---|---|---|
| 1 | 993 | 7 | 0.7 | –34 |
| 2 | 995 | 5 | 0.5 | –35 |
| 3 | 990 | 10 | 1.0 | –37 |
| 4 | 993 | 7 | 0.7 | –37 |
| 5 | 990 | 10 | 0.5 | –36 |
| 6 | 992 | 8 | 0.8 | –36 |
| 7 | 994 | 6 | 0.6 | –35 |
| 8 | 991 | 9 | 0.9 | –36 |

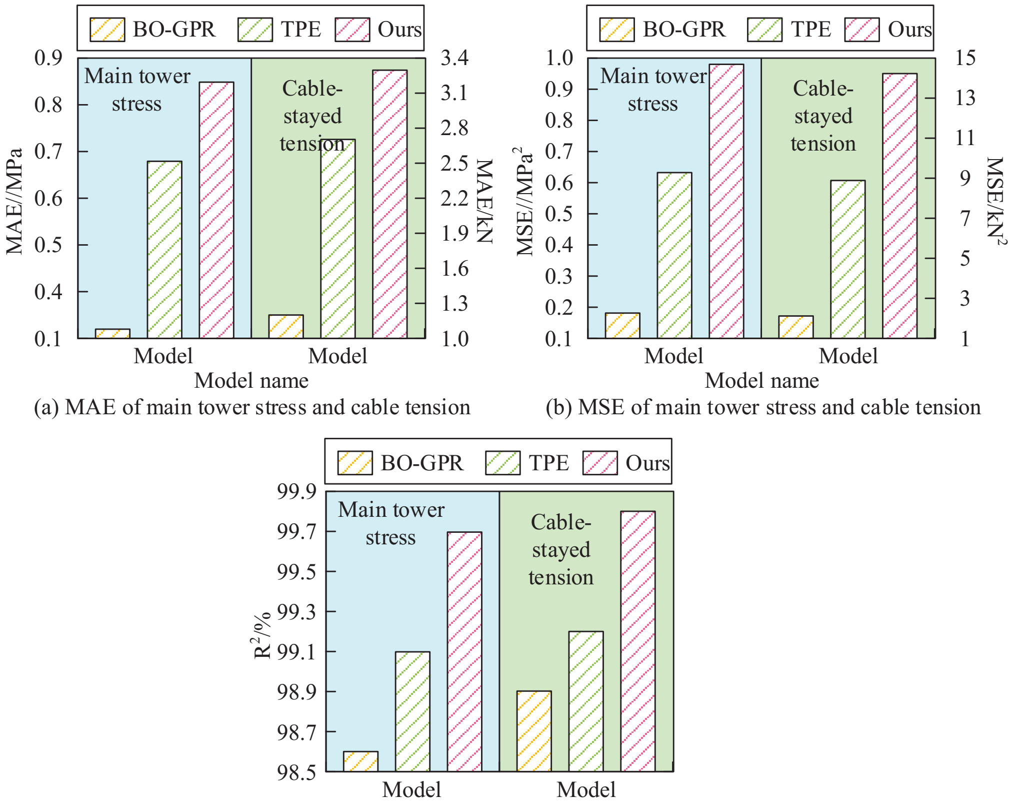

(a) MAE of main tower stress and cable tension
(b) MSE of main tower stress and cable tension
(c) $R^2$ of main tower stress and cable tension

**Fig. 9.** Comparison data of fitting accuracy among different models.

Table 2 showed that the packet loss rate in the eight repeated tests ranged from 0.5% to 1.0%, with an average of only 0.7125%. The RSSI remained stable between −34 and −37 dBm, with a fluctuation range of only 3 dBm. This indicated that the optimized WSN's communication performance met the monitoring requirements of railway CSBs under complex service environments. To verify the fitting ability of the fused WSN and MISSA-SVM models for the reliability indicators of railway CSBs, three indicators⊠ – mid-span deflection of the main girder, stress of the main tower, and tension of the stay cables – ⊠were selected as fitting objects. Finite element simulation data were used as the true values, and the fitting accuracy of MISSA-SVM, Bayesian optimization–Gaussian process regression (BO-GPR), and tree-structured Parzen estimator (TPE) was compared. The test selected 100 sets of sample data. The MAE, MSE, and coefficient of determination ($R^2$) were used as evaluation indicators. The comparison data of fitting accuracy was shown in Figure 9.

Figure 9a showed the MAE of the main tower stress and the cable tension. From Figure 9a, the MISSA-SVM model had a main tower stress MAE of only 0.32 MPa and a cable tension MAE of 1.2 kN, indicating the smallest fitting error. Figure 9b showed the MSE of the main tower stress and the

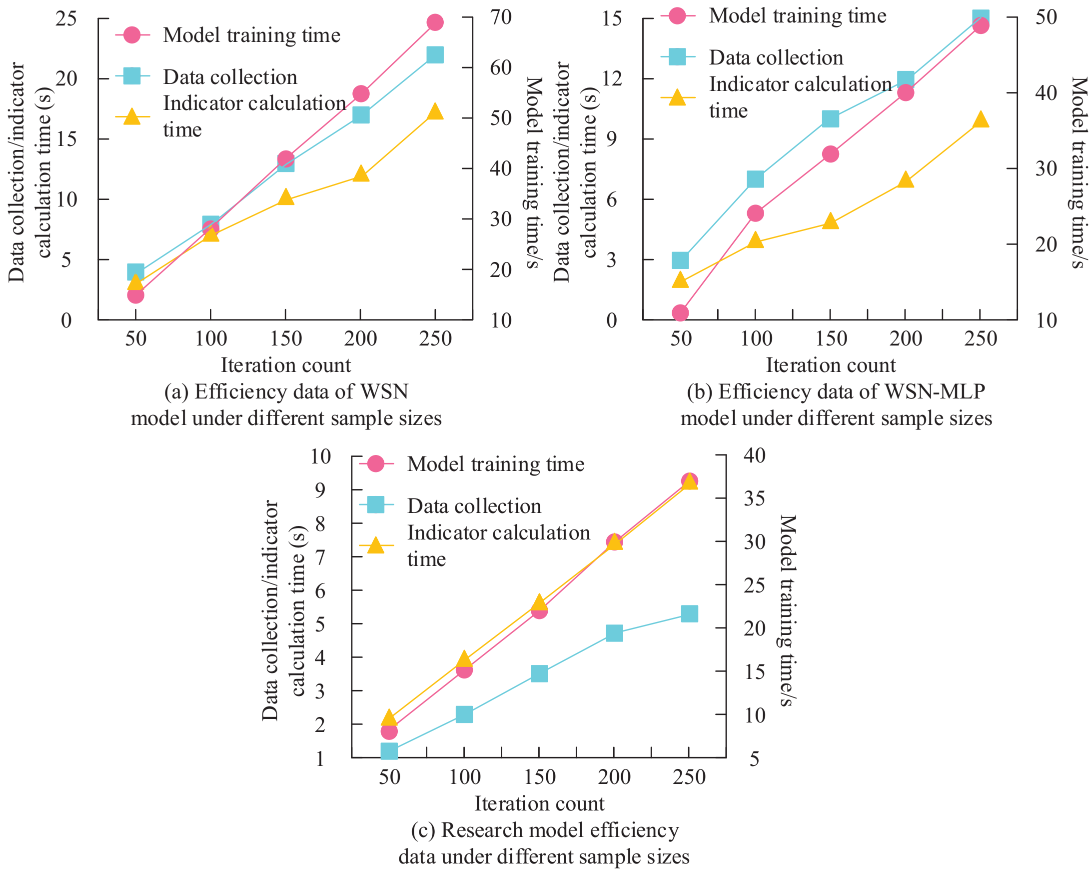


**Fig. 10.** Comparison data of model operation efficiency under different sample sizes.

cable tension. From Figure 9b, the main tower stress MSE was 0.18 $\mathrm{MPa}^2$ and the cable tension MSE was 2.1 $\mathrm{kN}^2$, indicating better fitting stability. Figure 9c shows the $R^2$ of the main tower stress and the cable tension. From Figure 9c, the MISSA-SVM model had the highest $R^2$ value, with $R^2$ values of 99.7% and 99.8% for the main tower stress and the cable tension, respectively. Compared with the TPE and BO-GPR models, the MISSA-SVM model effectively reduced the fitting error and improved the stability of the prediction results through parameter optimization. To verify the computational efficiency advantage of the proposed model, the study introduced the WSN-multilayer perceptron (WSN-MLP) model as a control. The computational efficiency comparison data of each model under different sample numbers was shown in Figure 10.

As shown in Figure 10a, as the sample size increased from 50 to 250 groups, the data acquisition time of the WSN model increased from 4 to 22 s, the model training time increased from 15 to 69 s, and the index calculation time increased from 3 to 17 s, with the total time increasing from 22 to 108 s, a significant increase. Figure 10b showed that with a sample size of 250 groups, the data acquisition, model training, and index calculation times for the WSN-MLP model were 15, 49, and 10 s, respectively. Figure 10c showed that the growth rate of the various time-consuming parameters of the research model was lower than that of the WSN model. With a sample size of 250 groups, the data acquisition, model training, and index calculation times were 5.3, 37, and 9.2 s, respectively, with a total time of only 51.5 s, a reduction of 52.3% compared with the WSN model. Overall, out of the total time-consuming aspect of the proposed model of 51.5 s, real-time data collection was only 5.3 s. The time consumption of model training and calculation was within a reasonable range, which met the real-time requirements of high-speed railway bridge health monitoring.

## 4 Conclusion

To address the pain points of low fitting accuracy and unreasonable node deployment in traditional railway CSB reliability assessment, a reliability assessment model combining WSN real-time sensing and MISSA-SVM collaboration was constructed. The model's performance was verified through theoretical design, simulation experiments, and field testing. The study found that the packet loss rate in eight repeated tests ranged from 0.5% to 1.0%, with an average of only 0.7125%, far below the commonly used threshold of 5% in industrial wireless communication. The RSSI remained stable between −34 and −37 dBm, with a fluctuation range of only 3 dBm. The optimized WSN node coverage reached 82%, effectively eliminating sensing blind spots. Regarding assessment accuracy and efficiency, the average absolute error of the main tower stress fitting was only 0.32 MPa, and the total computation time for 250 samples was 51.5 s. However, the study still has certain limitations. The MISSA still suffers from slowed convergence speed in ultrahigh-dimensional data processing scenarios. Future research could simplify the iterative process and improve the model's computational efficiency in ultra-high dimensional data scenarios.


## Funding

None.


## Conflicts of interest

The authors declare that they have no conflict of interest.

## Data availability statement

The datasets generated during and/or analyzed during the current study are available from the corresponding author on reasonable request.

## Author contribution statement

The sole author of this manuscript is responsible for the entire research process.

## References


1. V.T. Pham, D.K. Thai, S.E. Kim, A novel procedure for cable damage identification of cable-stayed bridge using particle swarm optimization and machine learning, Struct. Health Monit. **24**, 714–737 (2025)
2. A. Bayraktar, A. Erdiş, A. Kurşun, Y. Taş, M. Akköse, Impact-induced vibration effects on the real dynamic behaviour of cable-stayed bridges, Proc. Inst. Civ. Eng. Struct. Build. **177**, 359–370 (2024)
3. J. Yang, J. Huo, C. Mu, A novel clustering routing algorithm for bridge wireless sensor networks based on spatial model and multicriteria decision making, IEEE Internet Things J. **11**, 27775–27789 (2024)
4. L. Tan, Y. Liu, H. Zhang, T. Yuan, Z. Shang, X. Jiang, 3dSN-SSA: wireless sensor network deployment of 3D surface based on improved sparrow search algorithm, Wirel. Netw. **31**, 4637–4648 (2025)
5. M. Saxena, S. Dutta, B.K. Singh, Optimal routing using whale optimization and lion optimization algorithm in WSN, Wirel. Netw. **30**, 1601–1618 (2024)
6. G. Chen, H. Sun, Multi-strategy improved sparrow search algorithm based on first definition of ellipse and group co-evolutionary mechanism for engineering optimization problems, Cluster Comput. **27**, 14005–14035 (2024)
7. G. Chen, D. Zhu, X. Chen, Similarity detection method of science fiction painting based on multi-strategy improved sparrow search algorithm and Gaussian pyramid, Multimed. Tools Appl. **83**, 41597–41636 (2024)
8. C.E. Cukaci, S. Soyoz, Vision-based identification of cable tensions and finite element model verification of a cable-stayed bridge, J. Civ. Struct. Health Monit. **15**, 1319–1335 (2025)
9. M. Alrizq, S. Stalin, S. Alyami, V. Roy, A. Mishra, A.K. Chandanan, P. Venkatesh, Optimization of sensor node location utilizing artificial intelligence for mobile wireless sensor network, Wirel. Netw. **30**, 6619–6631 (2024)
10. N. Anusha, B.R. Tapas Bapu, S. Selvakumaran, A. Vijayaraj, C. Ramesh Kumar, P. Raji, Cyber intrusion detection using dual interactive Wasserstein generative adversarial network with war strategy optimization in wireless sensor networks, Multimed. Tools Appl. **84**, 19223–19253 (2025)
11. P. Kathiroli, S. Kanmani, Data aggregation by enhanced squirrel search optimization algorithm for in wireless sensor networks, Wirel. Netw. **31**, 2181–2201 (2025)
12. M.F.U.D. Afzal, A. Javed, Non-contact measurement of vibration modes of large cable-stayed bridge under ambient conditions: a convenient way of condition monitoring of bridges, J. Civ. Struct. Health Monit. **14**, 339–353 (2024)
13. A.A. Qaffas, Applying an improved squirrel search algorithm (ISSA) for clustering and low-energy routing in wireless sensor networks (WSNs), Mob. Netw. Appl. **29**, 1753–1768 (2024)
14. J. Wang, Z. Zhu, F. Zhang, Y. Liu, An improved salp swarm algorithm for solving node coverage optimization problem in WSN, Peer-to-Peer Netw. Appl. **17**, 1091–1102 (2024)
15. J. Guo, Y. Sun, T. Liu, Y. Li, T. Fei, An improved sparrow search algorithm and its application in wireless sensor node coverage problem, Int. J. Sens. Netw. **46**, 230–244 (2024)
16. S. Rabhi, Improving localization precision in wireless sensor networks using salp swarm algorithm, Optoelectron. Instrum. Data Process. **60**, 632–643 (2024)
17. K. Dinesh, S.K. Svn, GWO-SMSLO: Grey wolf optimization based clustering with secured modified Sea Lion optimization routing algorithm in wireless sensor networks, Peer-to-Peer Netw. Appl. **17**, 585–611 (2024)
18. L. Almuqren, N. Alruwais, A.A. Alhashmi, I.R. Alzahrani, N. Salih, M. Assiri, K. Shankar, WSN-assisted consumer purchasing power prediction via barracuda swarm optimization-driven deep learning for E-commerce systems, IEEE Trans. Consum. Electron. **70**, 1694–1701 (2024)
19. V. Kusla, G.S. Brar, MOBES: a modified bald eagle search based technique for optimal clustering in wireless sensor network, Univ. Politeh. Buchar. Sci. Bull. Ser. C Electr. Eng. Comput. Sci. **86**, 207–224 (2024)
20. L. Zhang, Y. Deng, J. Fu, L. Li, J. Hu, K. Di, A DV-Hop localization algorithm corrected based on multi-strategy sparrow algorithm in sea-surface wireless sensor networks, Wirel. Netw. **31**, 1405–1420 (2025)


**Cite this article as**: Liyan Xu, Construction of a reliability assessment model for railway cable-stayed bridges based on WSN real-time sensing and MISSA-SVM collaboration, Int. J. Metrol. Qual. Eng. **17**, 14 (2026), https://doi.org/10.1051/ijmqe/2026014